

1 **Modelling the occurrence of heat waves in maximum**
2 **and minimum temperatures over Spain and**
3 **projections for the period 2031-60**

4 **Abaurrea, J. · Asín, J. · Cebrián, A.C.**

5

6 Received: date / Accepted: date

7 **Abstract** The occurrence of extreme heat events in maximum and minimum daily
8 temperatures is modelled using a non homogeneous common Poisson shock pro-
9 cess. It is applied to five Spanish locations, representative of the most common
10 climates over the Iberian Peninsula. The model is based on an excess over thresh-
11 old approach and distinguishes three types of extreme events: only in maximum
12 temperature, only in minimum temperature and in both of them (simultaneous
13 events). It takes into account the dependence between the occurrence of extreme
14 events in both temperatures and its parameters are expressed as functions of time
15 and temperature related covariates. The fitted models allow us to characterise the
16 occurrence of extreme heat events and to compare their evolution in the different
17 climates during the observed period.

18 This model is also a useful tool for obtaining local projections of the occur-
19 rence rate of extreme heat events under climate change conditions, using the future
20 downscaled temperature trajectories generated by Earth System Models. The pro-

J. Abaurrea
University of Zaragoza

J. Asín
University of Zaragoza

A.C. Cebrián
University of Zaragoza
E-mail: acebrian@unizar.es

jections for 2031-60 under scenarios RCP4.5, RCP6.0 and RCP8.5 are obtained and analysed using the trajectories from four earth system models which have successfully passed a preliminary control analysis. Different graphical tools and summary measures of the projected daily intensities are used to quantify the climate change on a local scale. A high increase in the occurrence of extreme heat events, mainly in July and August, is projected in all the locations, all types of event and in the three scenarios, although in 2051-60 the increase is higher under RCP8.5. However, relevant differences are found between the evolution in the different climates and the types of event, with a specially high increase in the simultaneous ones.

Keywords Extreme heat events · non homogeneous Poisson process · bivariate models · climate projections · climate change

1 Introduction

The analysis of heat waves is an increasingly important issue due to the serious impact of this phenomenon on ecosystems, the economy and human health; see for example Beniston et al (2007), Barriopedro et al (2011), Amengual et al (2014) and Tobías et al (2014). There is no standard definition of heat wave and many authors, such as Perkins and Alexander (2013) and Smith et al (2013), address the issue of analysing different measurements and definitions of this phenomenon. Traditionally, heat waves have been defined using daily maximum temperatures but there is an increasing number of definitions including information on both maximum and minimum daily temperatures; see for example Tryhorn and Risbey (2006), Keellings and Waylen (2014) or the definition by the U.S. National Weather Service. According to Hajat et al (2006), both temperatures should be considered to analyse the effect of heat waves on human health.

The global warming induced by the increasing concentration of greenhouse gases in the atmosphere during the 20th century, and especially during its last decades, will probably continue. Many works, such as Meehl et al (2005), Tryhorn

49 and Risbey (2006) and Lemonsu et al (2014), suggest that heat waves will become
50 more frequent. In this context, an important issue for preventing global warming
51 impacts is the characterization and future projection, on a local scale, of heat
52 waves including information on both maximum and minimum daily temperatures.

53 Temperature projections at a daily and local scale are often required, see Wang
54 et al (2012), Casanueva et al (2013) and Lau and Nath (2014), who emphasise the
55 interest of using a fine spatial resolution to investigate regional phenomena. Nowa-
56 days, Earth System Models (ESMs) are the best tool for obtaining future projec-
57 tions of atmospheric variables on a monthly or seasonal scale over broad areas.
58 However, they are unable to provide reliable temperature trajectories on a daily
59 and local scale, and cannot be directly used to project the extreme temperature
60 behaviour of local daily series, see Yue et al (2016), Brands et al (2013), Cattiaux
61 et al (2013), and Keellings and Waylen (2015) who find that AR5 models are not
62 able to reproduce extremes over the 90th percentile. Regional Circulation Mod-
63 els (RCMs) neither guarantee an adequate reproduction of extreme temperature
64 events. For example, Vautard et al (2013), using the RCM projections driven by
65 ERA-Interim, find an overestimation of summer temperature extremes in Mediter-
66 ranean regions and an underestimation over Scandinavia. They also conclude that
67 the increase of the RCM resolution does not generally improve this deficiency.
68 Grotjahn et al (2016) conclude that dynamic methods overestimate the frequency
69 of heat waves and underestimate that of cold events.

70 In this context, the use of statistical models to obtain heat wave projections is
71 essential for many applications which require daily projections at a local spatial
72 scale, such as health studies linked to heat extremes in big cities and other climate
73 change impact studies. Another advantage of the statistical models is that they are
74 able to deal with non stationary situations, be it using non constant thresholds,
75 Kyselý et al (2010), or parameters depending on time or other covariates, see
76 Cheng et al (2014), García-Cueto et al (2014) and Abaurrea et al (2015b).

77 In this work, a bivariate point process, the common Poisson shock process,
78 is used to model the occurrence of extreme heat events (EHE) in maximum and
79 minimum daily temperatures. This model improves the univariate approaches,
80 such as those suggested by Abaurrea et al (2007), Furrer et al (2010) or Kyselý
81 et al (2010), since it takes into account the dependence between the occurrence
82 of extreme events in both temperatures. The model can be easily generalised to a
83 non stationary framework by making its parameters be a function of time-varying
84 covariates. Here, only temperature related covariates are considered but other type
85 of variables could also be used. An advantage of this model is that it can be easily
86 estimated using the R package NHPoisson, see Cebrián et al (2015).

87 The model can be used to obtain local projections of the occurrence rate of
88 EHEs under climate change conditions. These conditions are represented by co-
89 variates obtained from the future temperature trajectories generated by ESMS,
90 appropriately downscaled to fit the climate characteristics of the considered loca-
91 tion. Summary measures of these projected daily intensities allow us to quantify
92 the local climate change.

93 The methodology is summarised in Section 2. Section 3 describes the data: the
94 temperature series from five Spanish locations and four ESM daily trajectories.
95 Section 4 shows and compares the fitted models in these locations. In Section 5,
96 projections under scenarios RCP4.5, RCP6.0 and RCP8.5 for the period 2031-60
97 are obtained and analysed. Section 6 summarises the most relevant conclusions.

98 **2 Methodology**

99 2.1 Modelling the occurrence of extreme heat events

100 *Common Poisson shock process* The modelling of extreme events in environmen-
101 tal sciences is often based on the excess over threshold (EOT) approach, where an
102 extreme event is defined as a run of observations whose values exceed a reference
103 threshold; see Coles (2001). There is a point process characterization of extreme

104 value models which states that, under mild conditions and if the threshold is ex-
105 tremely enough, the occurrence of the extreme events follows a Poisson process.
106 Since a heat wave may provoke extreme values both in maximum and minimum
107 daily temperatures, a bivariate approach will improve the univariate models usu-
108 ally applied to characterize the occurrence of EHEs. In particular, a bivariate point
109 process with dependent marginal processes is a reasonable framework to jointly
110 model the occurrence of EHEs. In this work, a common Poisson shock process
111 (CPSP) is considered; see Abaurrea et al (2015b) for a full justification of this
112 model. One of the advantages of this approach is that it can be easily adapted to
113 non stationarity.

114 A bivariate CPSP assumes that there is an underlying Poisson process (PP) of
115 shocks N_0 that can yield two different types of events. The counting processes of
116 each type of event are the marginal processes N_1 and N_2 . The CPSP assumes that
117 dependence occurs by the simultaneity of the events, so that it can be decomposed
118 into three independent indicator PPs $N_{(1)}$, $N_{(2)}$ and $N_{(12)}$, which include the
119 events occurring only in process N_1 , only in N_2 , and those occurring simultaneously
120 in both of them. Their intensities are denoted $\lambda_{(1)}$, $\lambda_{(2)}$ and $\lambda_{(12)}$, respectively,
121 so that the intensities of the marginal processes $N_1 = N_{(1)} + N_{(12)}$ and $N_2 =$
122 $N_{(2)} + N_{(12)}$ are $\lambda_1 = \lambda_{(1)} + \lambda_{(12)}$ and $\lambda_2 = \lambda_{(2)} + \lambda_{(12)}$.

123 The CPSP can be generalised to the nonhomogeneous case, by allowing the
124 indicator intensities to be a function of a vector of time-varying predictors $\mathbf{x}(t)$
125 and using a logarithmic link, $\lambda(t|\mathbf{x}(t)) = \exp(\beta' \mathbf{x}(t))$. The predictors also help to
126 model the dependence induced by the systematic part of the three intensities.

127 The estimation of this model reduces to the estimation of three independent
128 nonhomogeneous PPs, which can be carried out by maximum likelihood, and the
129 covariate selection by a forward approach based on likelihood ratio tests. A detailed
130 example of the estimation of a nonhomogeneous PP can be found in Abaurrea
131 et al (2007) and it can be easily implemented using the R package, NHPPoisson,
132 previously mentioned.

133 *Definition of extreme heat events* The use of the CPSP for modelling EHEs in
 134 maximum and minimum daily temperature series (Tx_t and Tn_t herein) requires
 135 some previous operational definitions. In particular, the three indicator processes
 136 and the types of extreme events whose occurrence is modelled in each process
 137 have to be defined: $N_{(1)}$ is the process which includes the EHEs only in Tx_t , $N_{(2)}$
 138 includes the EHEs only in Tn_t , and $N_{(12)}$ those occurring simultaneously in both
 139 temperatures. Following the EOT definition of extreme event, an EHE only in Tx_t
 140 is a run of consecutive days where Tx_t exceeds U_x but Tn_t does not exceed U_n ,
 141 being U_x and U_n the extreme thresholds of the corresponding temperature series.
 142 An EHE only in Tn_t is defined analogously, and a simultaneous EHE is a run of
 143 observations with Tx_t and Tn_t exceeding U_x and U_n , respectively.

144 *Predictors* Since the final objective of the model is to obtain future projections of
 145 the occurrence of EHEs, only variables with reliable future projections should be
 146 considered as potential predictors. Three types of variables are used here.

- 147 • **Seasonal terms:** Given that temperature series show a seasonal behaviour,
 148 seasonal terms have to be included in the model. In this case, they are defined
 149 as the part of the annual harmonic signals corresponding to the period of the
 150 year under consideration.
- 151 • **Short moving averages of temperature:** The moving average of Tx_t and
 152 Tn_t in 15 or 31 day intervals around t , denoted by Tx_{m15} , Tn_{m15} , Tx_{m31}
 153 and Tn_{m31} , and their corresponding polynomial terms are considered. The
 154 reason to use these signals is that the projections provided by ESMs of the
 155 temperature series on an aggregated time scale of 15 or more days are reliable,
 156 while the projections of daily temperatures are not.
- 157 • **Interaction terms:** Interaction terms between the harmonic and the temper-
 158 ature predictors.

159 *Validation analysis.* The assumptions to be checked in a CPSP model are that
 160 the three indicator processes are non homogeneous PPs mutually independent.

161 The first assumption is checked using the Kolmogorov-Smirnov (KS) test for the
162 distribution of the residuals, and the Pearson test for serial correlation. The inde-
163 pendence assumption is checked with the bootstrap test developed by Abaurrea
164 et al (2015a). The details of the validation techniques can be found in Abaurrea
165 et al (2015b).

166 2.2 Projection of the extreme events

167 Once a suitable model is fitted, the projection of the occurrence of EHEs is ob-
168 tained using as input the covariates built from the future temperature trajectories
169 provided by the ESMs. It is noteworthy that the ESM trajectories have to be
170 properly downscaled to fit the site climate characteristics, before using them as
171 input. In effect, statistical downscaling procedures bridge the gap between the
172 ESM output, which are averages in gridcells with areas larger than $1^\circ \times 1^\circ$, and
173 the information at a local scale required by the model, see Gutiérrez et al (2013).
174 In addition, a validation analysis of the quality of the downscaled ESM trajectories
175 should be carried out before using them for projecting.

176 **Validating a trajectory.** Two aspects are considered in the validation anal-
177 ysis. The first is that the downscaled ESM trajectory in the historical scenario
178 reproduces satisfactorily the distribution of the observed temperatures, in par-
179 ticular, its tail distribution. Three tools are suggested to check this assumption:
180 two exploratory graphs, see Section 5.1.1, and the test developed by Rosenbaum
181 (2005), which checks the equality of two multivariate distributions. This require-
182 ment is not fulfilled by the temperature variables on a daily scale, as previously
183 mentioned.

184 The second aspect is a control to avoid extrapolation. In a statistical model,
185 the values of the covariates used to obtain predictions, in this case the future
186 downscaled ESM trajectories, should not extrapolate the range of values used
187 to fit the model. In particular, the reason why decadal temperature trends have
188 not been considered as potential covariates, is that most of the values of their

189 future projections lead to extrapolation problems. That is also the reason why only
190 medium-term projections can be obtained using short moving average temperature
191 variables.

192 3 Data

193 3.1 Observed data

194 The daily maximum and minimum temperature series, measured in $^{\circ}C$, of five
195 Spanish locations (Zaragoza, Barcelona, Badajoz, Albacete and Burgos) are anal-
196 ysed in this work. These series have been provided by the Spanish meteorological
197 agency, AEMET. Their geographical position and Köppen¹ climate classification
198 are shown in Figure 1. Three of the series are located in the northern half of Spain:
199 Burgos with a Cfb climate, Barcelona sited on the Mediterranean coast with a Csa
200 climate and Zaragoza, in the Ebro valley, with a transition climate between the
201 previous two, Bsk. Albacete and Badajoz are located in the southern half, in the
202 Mediterranean and Atlantic slopes, with Bsk and Csa climates, respectively. These

¹ <http://es.climate-dat.org/location/3316>

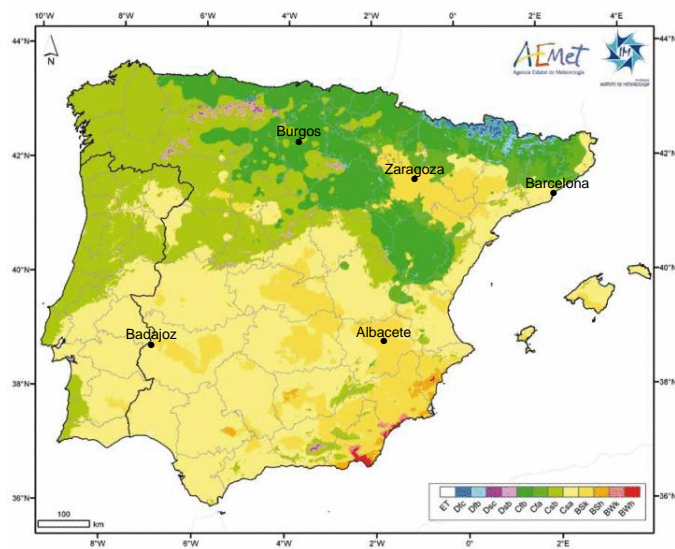


Fig. 1 Köppen classification and localization of the analysed series. Map from AEMET (2011).

203 locations represent the most common climates in the Iberian Peninsula. It was no
204 possible to analyse other climates since series of the required length and quality
205 were not available.

206 In the Iberian peninsula summer runs from June to September, and an EHE has
207 never been observed before May or after September. Consequently, the analysis of
208 the occurrence of EHEs can be restricted to these months (MJJAS). The thresholds
209 U_x and U_n used to characterize the EHEs in Tx_t and Tn_t are usually defined as
210 percentiles of the observed series. The most common value is the 90th percentile,
211 see for example Tryhorn and Risbey (2006), but values between the 90th and 99th
212 percentiles are also frequently used, see Hajat et al (2006). Since only Spanish
213 series are considered in this work, and AEMET (2011) defines heat waves using as
214 threshold the 95th percentile of the daily temperature series from July to August
215 in the reference period 1971-2000, that percentile is used to define U_x and U_n .

216 Some characteristics of the Tx_t and Tn_t series are summarised in the first rows
217 of Table 1: the altitude of the station, the record periods of Tx_t and Tn_t and their
218 means in June, July, August and in the period MJJAS. The thresholds U_x and
219 U_n are shown in the bottom part of Table 1, together with the observed number
220 of EHEs in each indicator process.

221

222 3.2 ESM Data

223 Four CMIP5 climate models are used in this work, MPI-ESM-LR (MPI in short),
224 CanESM2 (CE2), IPSL-CM5A-MR (IPSL) y MRI-CGCM3 (MRI). They are cho-
225 sen for the quality of its representation of the summer climate patterns in the
226 Atlantic area close to the Iberian Peninsula, among the CMIP5 models evaluated
227 by Sánchez de Cos et al (2016).

228 Representative Concentration Pathways (RCPs) are greenhouse gas concen-
229 tration trajectories which are consistent with a wide range of possible changes in
230 future anthropogenic greenhouse gas emissions. In this work, three scenarios are

Series	Zaragoza	Barcelona	Badajoz	Albacete	Burgos
Altitude (m. a.s.l.)	263	412	185	702	891
Record period	1951-2005	1951-2005	1955-2005	1961-2005	1971-2008
$\overline{T_{x_t}}$ MJJAS	28.1	24.7	30.8	28.5	23.5
$\overline{T_{x_t}}$ Jn	27.7	24.1	30.3	27.9	22.0
$\overline{T_{x_t}}$ Jl	31.5	27.8	34.3	32.5	26.4
$\overline{T_{x_t}}$ Au	31.0	27.6	34.0	31.9	26.7
$\overline{T_{n_t}}$ MJJAS	15.1	16.3	14.9	13.3	9.1
$\overline{T_{n_t}}$ Jn	14.8	15.3	14.7	12.7	8.5
$\overline{T_{n_t}}$ Jl	17.6	18.6	17.0	16.0	11.0
$\overline{T_{n_t}}$ Au	17.8	18.7	16.7	16.1	11.1
U_x	37.0	31.8	39.6	37.0	33.2
U_n	21.2	22.0	20.6	19.4	14.8
# EHE $N_{(1)}$	120	97	93	89	80
# EHE $N_{(2)}$	92	114	124	117	89
# EHE $N_{(12)}$	58	82	51	38	22

Table 1 Summary values of T_{x_t} and T_{n_t} series (in $^{\circ}C$), thresholds U_x and U_n used to define EHEs, and number of EHEs in each indicator process.

231 considered: RCP4.5 where emissions peak around 2040 and then decline, RCP6.0
232 where emissions peak around 2080 and then decline, and RCP8.5 where emissions
233 continue to rise throughout the 21st century. These scenarios are the most com-
234 monly used in climate change works, see Lau and Nath (2014) and Pereira et al
235 (2017) for example, and they cover a range of different future scenarios from less
236 to more pessimistic situations.

237 AEMET provides in its webpage ², the downscaled temperature series from
238 more than 20 ESMs for different Spanish locations under scenarios RCP4.5 and
239 RCP8.5 and in two of the ESMs also under RCP6.0. They are downscaled using a
240 statistical procedure based on the regression method SDSM, see Wilby and Dawson
241 (2013). In this work, the downscaled daily T_x and T_n trajectories of the previ-
242 ously described locations, Albacete, Badajoz, Barcelona, Burgos and Zaragoza,
243 are needed. All of them, except Zaragoza, can be downloaded from the previous
244 webpage. In that case, Leciñena series, around 35km from Zaragoza, has been used
245 after transforming it by correcting the mean level and the variability biases. Only

² http://www.aemet.es/es/serviciosclimaticos/cambio_climat/datos_diarios

Loc	Mod	Tx_{m15}	Tx_{m31}	Tn_{m15}	Tn_{m31}	# par	R^2	KS	PC	Ipv
Zar	$N_{(1)}$	0.08		0.22		7	69	0.53	0.50	0.28
	I			0.25 0.12						
	$N_{(2)}$		-0.02	0.11		5	70	0.20	0.63	
	$N_{(12)}$		0.04	0.05		5	64	0.93	0.12	
Bar	$N_{(1)}$	0.86			-0.02	6	75	0.39	0.28	0.62
	Q	0.001								
	$N_{(2)}$			0.63	-0.03	6	46	0.40	0.97	
	Q			0.001						
	$N_{(12)}$	0.03		0.10	-0.06	6	73	0.62	0.60	
Bad	$N_{(1)}$	0.30				6	36	0.47	0.78	0.55
	I	0.23 0.13								
	$N_{(2)}$			0.30		6	35	0.06	0.62	
	I			0.22 0.11						
	$N_{(12)}$	0.04		0.06		5	78	0.27	0.70	
Alb	$N_{(1)}$	0.09		-0.03		5	41	0.18	0.60	0.24
	$N_{(2)}$			0.10		4	61	0.31	0.26	
	$N_{(12)}$	0.047				6	41	0.60	0.00	
	Q				1.35 0.004					
Bur	$N_{(1)}$		0.03	0.26		6	67	0.56	0.08	0.31
	Q			0.001						
	$N_{(2)}$			0.17		6	55	0.19	0.25	
	I			0.09 0.06						
	$N_{(12)}$	0.04		0.02		5	65	0.13	0.17	

Table 2 Coefficients of the temperature covariates; interaction terms between the corresponding covariate and the harmonic, and quadratic terms are labeled I and Q , respectively. Last columns: # par, the number of model parameters, R^2 (in %), and p-values of the KS test, the Pearson correlation test and the independence test.

246 two ESMs, IPSL and MRI, have projections for the scenario RCP6.0, so that only
 247 two trajectories are available in that case.

248

249 4 Fitted Models

250 A detailed example of the modelling process of a CPSP can be found in Abaurrea
 251 et al (2015b). The final models obtained following that approach are summarised
 252 in Table 2, where the coefficients of the significant temperature covariates are
 253 shown in the first columns. The rows labeled as I correspond to the interaction
 254 terms between the corresponding covariate and the harmonic, and those labeled

255 as Q to the quadratic term of the temperature variables. The fitted models are
 256 quite simple, with between 4 and 7 parameters. The linear predictors of the three
 257 indicator processes $N_{(1)}$, $N_{(2)}$ and $N_{(12)}$ include, in all the locations, an intercept
 258 and one harmonic term. Only four, out of 15 fitted models, include a significant
 259 interaction term, and another four include a quadratic temperature term. As ex-
 260 pected, the covariates based on 15-day moving averages are usually preferred over
 261 the 31-day averages.

262 At least one covariate related to Tx_t and another to Tn_t are significant in
 263 the $N_{(1)}$ models, except in Badajoz whose model only includes Tx_{m15} and its
 264 interaction. The Tx_t terms have an increasing effect in all the locations, since even
 265 the quadratic effect in Barcelona is positive in the observed temperature range.
 266 High values of Tn_t (greater than 12°C in Burgos due to the quadratic term) lead
 267 to a reduction of the events in $N_{(1)}$, except in Zaragoza where the harmonic term
 268 gives a positive slope from the 10th July. This reduction can be explained by the
 269 fact that high Tn_t temperatures lead to an increase in the simultaneous events.

270 All the $N_{(2)}$ models include at least one Tn_t term, but only Zaragoza requires
 271 a covariate related to Tx_t . The effect of Tn_t in all the locations increases the
 272 intensity in the observed temperature range, even the harmonic term in Badajoz
 273 and Burgos and the quadratic effect in Barcelona.

274 At least one covariate related to Tx_t and another to Tn_t are significant in the
 275 $N_{(12)}$ models. All the Tx_t terms have a positive linear trend while the effect of the
 276 Tn_t terms is also positive but not always linear.

277 The main results of the validation analysis are summarised in the last columns
 278 of Table 2: R^2 (the square correlation coefficient between the empirical and the
 279 fitted intensities), and the p-values of the KS, Pearson and the independence test,
 280 (see Section 2.1). All the models pass the validation analysis, and R^2 varies from 35
 281 to 78%. This coefficient is greater than 50 in 67% of the models. The empirical and
 282 fitted intensities, accumulated in periods of 5 months, are graphically compared

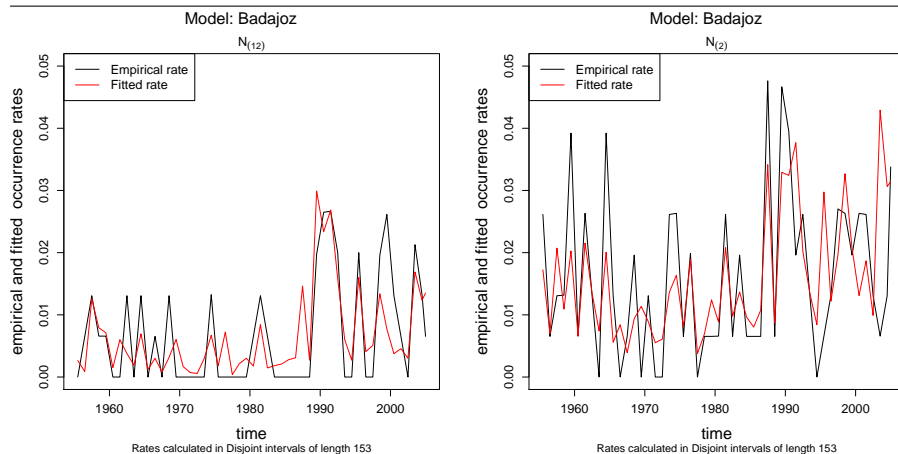


Fig. 2 Empirical and fitted intensities in Badajoz (models with the best and the worst fit).

283 with satisfactory results. As an example, the plots for the models with the best
 284 and the worst fit, Badajoz $N_{(12)}$ and $N_{(2)}$ respectively, are shown in Figure 2.

285 Figure 3 shows the LOWESS (with a 75 month window) of the three fitted
 286 intensities; for a better comparison the same y-scale is used in the three plots.
 287 A clear increase is observed from around the 90s in all the locations and types
 288 of event. Burgos shows one of the highest intensities in the tree types of event,
 289 while Zaragoza and Albacete are among the lowest. The high intensity of the
 290 simultaneous events in Barcelona is noteworthy. The greatest spatial variability is
 291 observed in $N_{(2)}$, with intensities in Burgos and Badajoz which are around four
 292 times the values in Zaragoza. The intensities of the three indicator processes show
 293 different levels. In all the locations, the highest intensities correspond to $N_{(2)}$, the
 294 medium ones to $N_{(1)}$ and the lowest to $N_{(12)}$, except for Zaragoza where the order
 295 of $N_{(2)}$ and $N_{(1)}$ is reversed.

296 5 ESM projections

297 In this section we obtain the projections under scenarios RCP4.5, RCP6.0 and
 298 RCP8.5 for the period 2031-60 using the ESM trajectories described in Section
 299 3.2 and the fitted models discussed in Section 4.

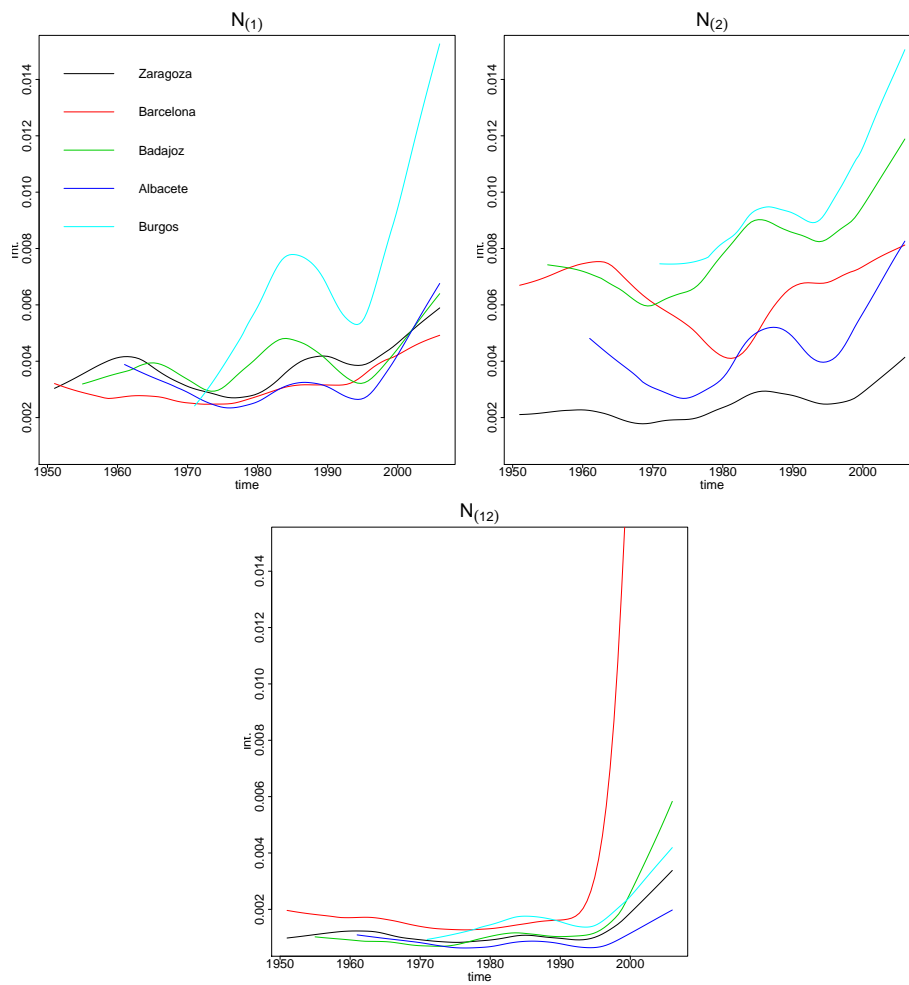


Fig. 3 Smoothed fitted intensities of the indicator processes. The y-scale in the plot for $N_{(12)}$ has been truncated from 0.05 (the maximum intensity in Barcelona) to 0.014.

300 5.1 Validating the trajectories

301 5.1.1 Checking the ESM performance under the current climate conditions

302 To check the performance of an ESM trajectory under the current climate condi-
 303 tions, the intensities fitted with the observed covariates are compared with those
 304 fitted with the corresponding downscaled historical trajectory. Since high inten-
 305 sities are of main interest, the comparison focuses on the high tails of the dis-

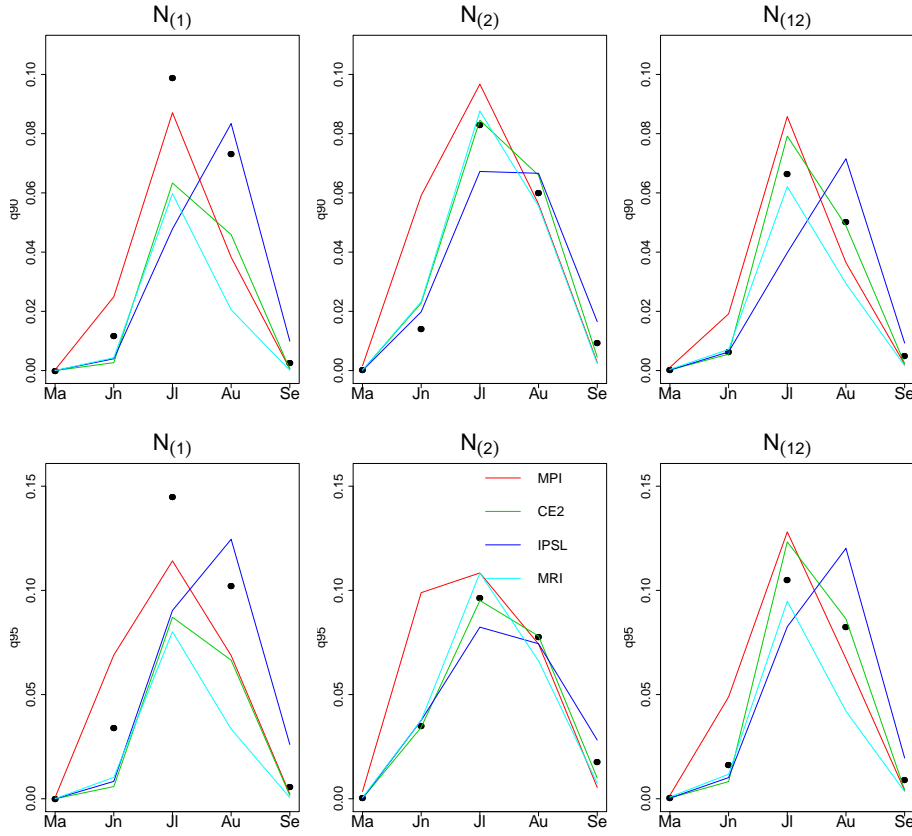


Fig. 4 Comparison of the observed (black points) and ESM percentiles for the historical scenario (lines), 90th percentile (top row) and 95th percentile (bottom row), Barcelona.

306 tributions, using two plots and a test. Given the seasonal character of the EHE
 307 occurrence, this analysis is carried out separately for each month.

308 The first plot compares the percentiles of the intensities fitted with the ob-
 309 served covariates (observed percentiles herein) with those obtained from the avail-
 310 able downscaled ESM trajectories (ESM percentiles). The plots for the 90th and
 311 95th percentiles (q_{90} and q_{95}) of the indicator models in Barcelona, shown as an
 312 example in Figure 4, are satisfactory.

313 The boxplots of the observed and the ESM 95th percentiles, by month, are
 314 used to check the inter-annual variability of the highest intensities. Each boxplot is
 315 based on a sample of 30 percentiles, one for each year during 1971-2000. The plots

316 for Barcelona, Figure 5, show that the ESM historical scenarios are compatible
317 with the observed ones. The dispersion of CE2 in May and June is much higher
318 than the other ESMs, in the three types of events. The same applies to MPI in
319 September.

320 Finally, the Rosenbaum test is applied to compare the observed and the ESM
321 bivariate distribution of the 90th and the 95th percentiles. A comparison for each
322 available trajectory and month is applied, using the same samples as in the previ-
323 ous boxplots. The results show that only 3% of the 300 trajectories (5 months \times
324 4 ESM \times 5 locations \times 3 types of events) are rejected at an $\alpha = 0.05$ significance
325 level, and 8% at $\alpha = 0.1$. It is concluded that the downscaled ESM trajectories
326 in historical scenarios reproduce satisfactorily the observed distributions, so that
327 their future counterparts can be used to project the three types of event in all the
328 locations.

329 *5.1.2 Checking extrapolation in future trajectories*

330 An extrapolation check of the covariates is essential since, under climate change
331 conditions, the cloud of points defined by the future covariates can be significantly
332 shifted with respect to the observed one, used to fit the model. As in any statistical
333 model, a frequent extrapolation may lead to unreliable projections.

334 Both marginal and multivariate extrapolation conditions are checked following
335 the approach by Abaurrea et al (2015b). Briefly, given a trajectory, the intensity
336 in day t , $\hat{\lambda}_t$, is obtained only if the values in that day of all the predictors are lower
337 than their corresponding maxima in the fitting period (marginal checking). Addi-
338 tionally, the Mahalanobis distance of the vector of predictors in t (with respect to
339 the observed mean vector and covariance matrix) must be lower than the maxi-
340 mum of the Mahalanobis distances in the fitting sample or, alternatively, all the
341 predictor values in t must be lower than their 90th percentiles in the fitting period
342 (multivariate checking). If the percentage of days not projected in a trajectory is
343 greater than 25%, it is removed from the analysis.

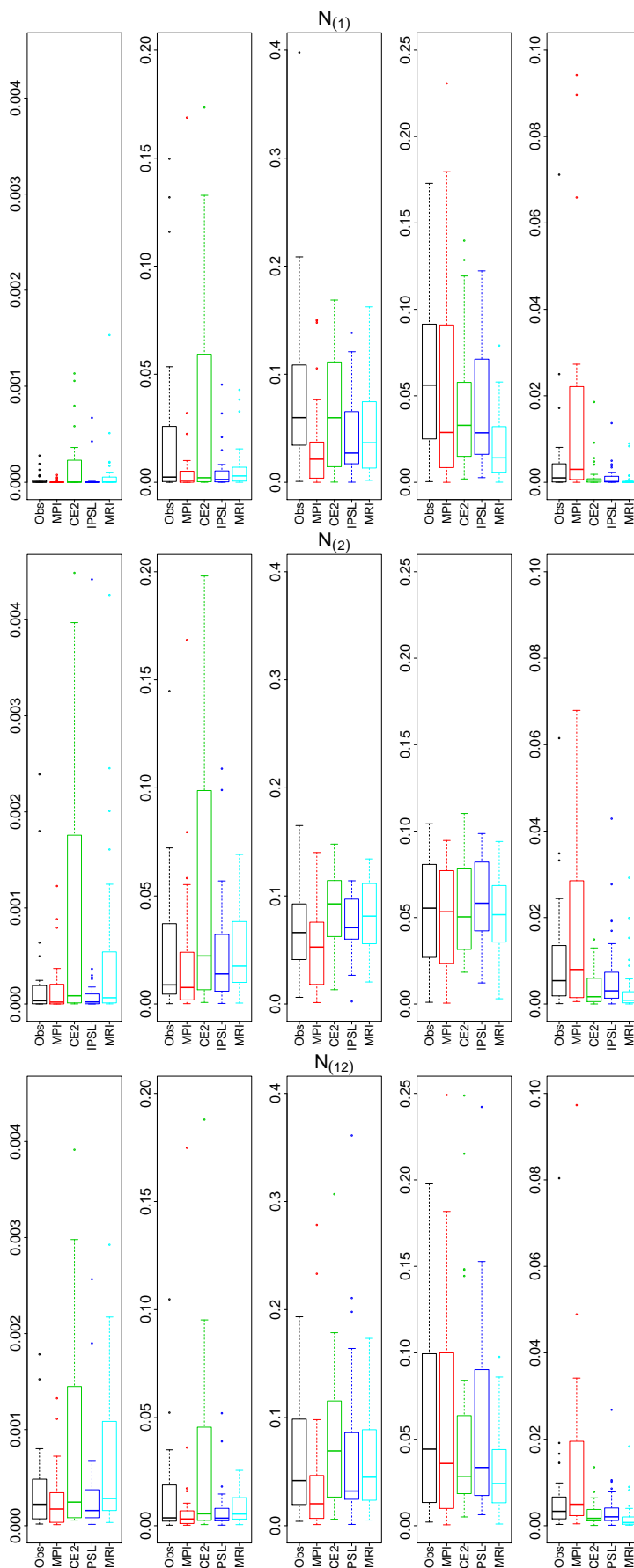


Fig. 5 Boxplots of the annual 95th percentiles calculated with the observed and the ESM trajectories in the historical scenario, 1971-2000, Barcelona.

# traj.	RCP4.5 (4 traj)	RCP6.0 (2 traj)	RCP8.5 (4 traj)
≥ 3	86.2%	0%	77.3%
1	4.0%	3.1%	9.3%
none	1.8%	3.6%	5.3%
(31-40)		Alb: Jl, Au, $N_{(12)}$	Alb: Au, $N_{(12)}$
(41-50)	Alb: Jl, $N_{(1)}$, $N_{(12)}$; Au, $N_{(12)}$		Alb: Jl, all $N_{()}$; Au, $N_{(1)}$, $N_{(12)}$
(51-60)	Alb: Jl, $N_{(12)}$	Alb: Jl, Au, all $N_{()}$	Alb: Jl, Au, all $N_{()}$

Table 3 Percentage of periods (from 225) where three or more (≥ 3), only one (1) or none of the available trajectories are projected. The location, month and indicator processes with no projection in each decade are indicated in the last three rows.

%	RCP4.5 (100)			RCP6.0 (50)			RCP8.5 (100)		
	$N_{(1)}$	$N_{(2)}$	$N_{(12)}$	$N_{(1)}$	$N_{(2)}$	$N_{(12)}$	$N_{(1)}$	$N_{(2)}$	$N_{(12)}$
2031-40	5	7	9	2	2	8	10	10	12
2041-50	10	12	13	2	0	2	16	19	15
2051-60	10	10	11	10	10	10	30	34	25

Table 4 Percentage of non projected periods by decade. The total number of periods is in round brackets.

344 Extrapolation is not a big problem except in Albacete, where projections in
345 July and August cannot be obtained. Table 3 shows the percentages from the 225
346 considered periods (5 months \times 3 decades \times 3 types of event \times 5 locations) where
347 three or more, only one, or none of the available trajectories are projected. Given
348 that 2 to 4 trajectories were initially available, the results are satisfactory.

349

350 To analyse the time evolution of the extrapolation problem, Table 4 summarises
351 the percentage of non projected periods by decade and type of event. A total of
352 100 periods (5 months \times 4 trajectories \times 5 locations) are available under RCP4.5
353 and RCP8.5, and 50 (5 \times 2 \times 5) under RCP6. The maximum percentages under
354 RCP4.5 and RCP6.0 are 13 and 10% respectively. Under the more severe RCP8.5
355 the percentages increase in the third decade with a maximum value of 34% non
356 projected periods.

357 5.1.3 Summary measures to analyse the projections

358 In each location, the fitted model provides the projected intensity in each day
359 in MJJAS for the period 2031-60 (4590 days), under three RCPs and for 2 to

360 4 trajectories. To deal with this huge amount of values, and since the aim is to
361 study the general evolution of the EHE occurrence, summaries of the projected
362 daily intensities are calculated. Robust summary measures are used to minimise
363 the effect of the projections obtained under some extrapolation.

364 To study the mean evolution of the projected intensities, we use the 25%
365 trimmed mean $\bar{\lambda}_{25}$ by month and decade, which is the mean of the daily intensities
366 once the lowest 25% and the highest 25% values are discarded. To study the vari-
367 ability, the interquartile range IQR_{λ} is used. Since 2 to 4 trajectories are available
368 in each location, the corresponding $\bar{\lambda}_{25}$ values of each model are summarised by
369 their median value, $Q2_{\bar{\lambda}_{25}}$ herein. These summary measures allow us to study the
370 seasonal behaviour and the time evolution of the projected intensities of each type
371 of event in each RCP, for the considered spatial area.

372 5.2 Projections 2031-60 under scenario RCP4.5

373 A detailed analysis of the projections obtained under RCP4.5 is shown in this
374 section, and a comparison with the results under RCP6.0 and RCP8.5, in the next
375 one.

376 As it was shown in Section 5.1.2 projections for Albacete could be obtained
377 only for a few periods, and not in July and August. For that reason, the results for
378 Albacete are not included in the figures of the following sections, although they
379 are summarized in the tables.

380 *Global analysis* To analyse the global behaviour of the projected intensities over
381 the area under study, the distribution of $\bar{\lambda}_{25}$ for all the trajectories in the four
382 locations is summarised using boxplots, see Figure 6. The boxplots are displayed
383 without the outliers to keep the y-scale short. As a reference, the minimum and
384 maximum of the observed trimmed means in the four locations are plotted as
385 horizontal lines.

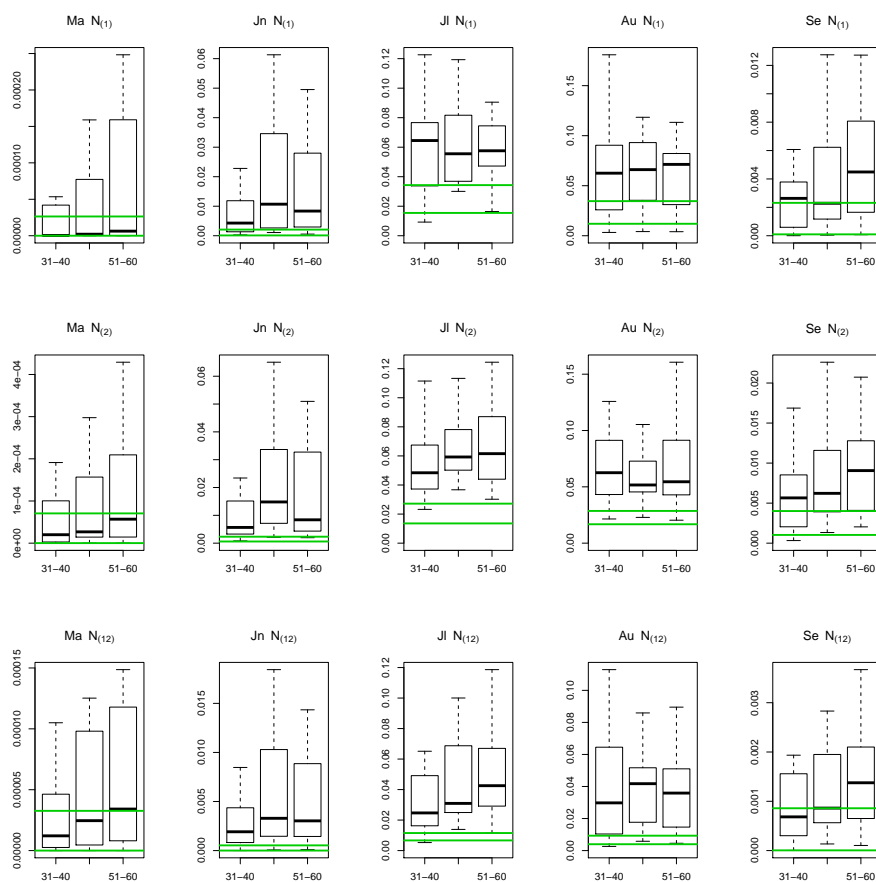


Fig. 6 Boxplots of the projected trimmed means $\bar{\lambda}_{25}$ in the four locations and all the trajectories available under RCP4.5. Green horizontal lines are the minimum and maximum of the observed $\bar{\lambda}_{25}$.

386 The maximum of the projected values in May is always lower than 0.0004. Since
 387 projections in this month do not lead to a relevant increase in the occurrence of
 388 EHEs and their impact is low, May will not be considered in the following analysis.

389 The boxplots show that the observed $\bar{\lambda}_{25}$ values from June to August are
 390 always lower than the 50th percentile of the corresponding projected $\bar{\lambda}_{25}$ and, in
 391 most cases, than the 25th percentile. This fact indicates a high agreement between
 392 the different ESMs in the projection of an important increase of the three types
 393 of events. In May, June and September this variability is lower in 2031-40 than

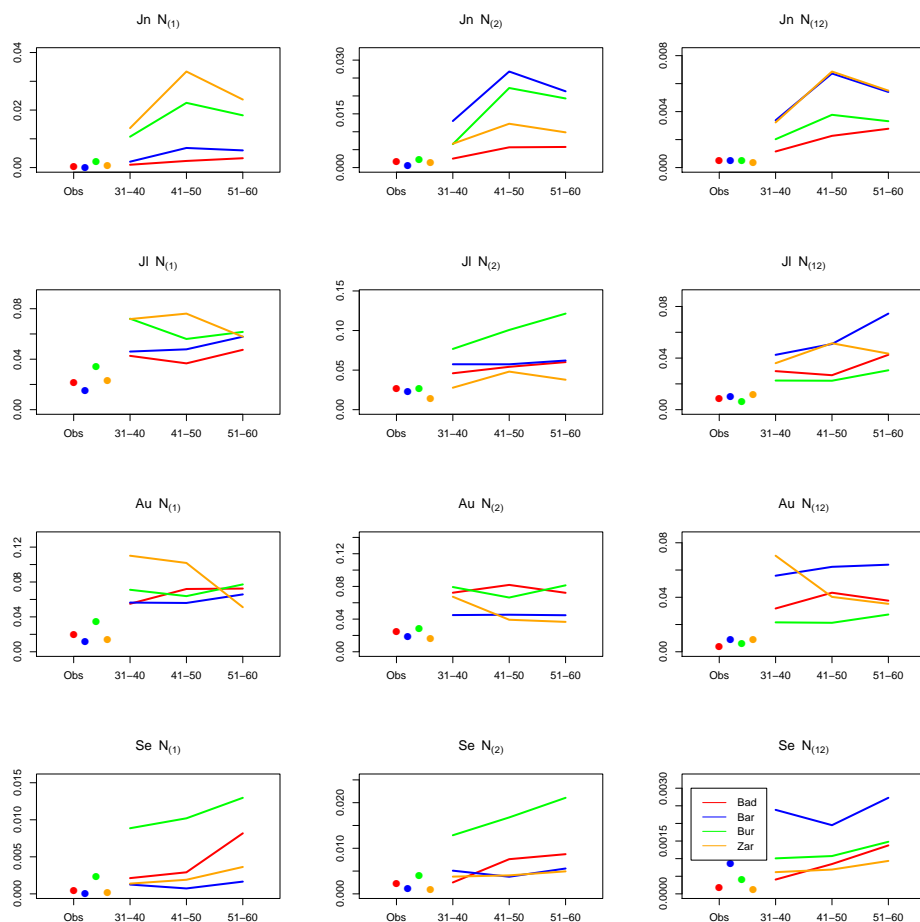


Fig. 7 Plots, by month and type of event, of Q_2 under RCP4.5 in the three decades and $\bar{\lambda}_{25}$ of the observed period. The projections of each location are displayed with different colours.

394 in the other decades. Since the variability comes from the different locations and
 395 trajectories, it means that the projections for the different locations and ESMs are
 396 more homogeneous in the first decade than later.

397 *Time evolution* To summarise and compare the time evolution of the mean level
 398 of the projections, Figure 7 shows Q_2 in the three decades and, as a reference
 399 value, the observed $\bar{\lambda}_{25}$. Most of the projected values increase from 2031-40 to
 400 2051-60, although this growth is not monotonous. It is noteworthy the case of

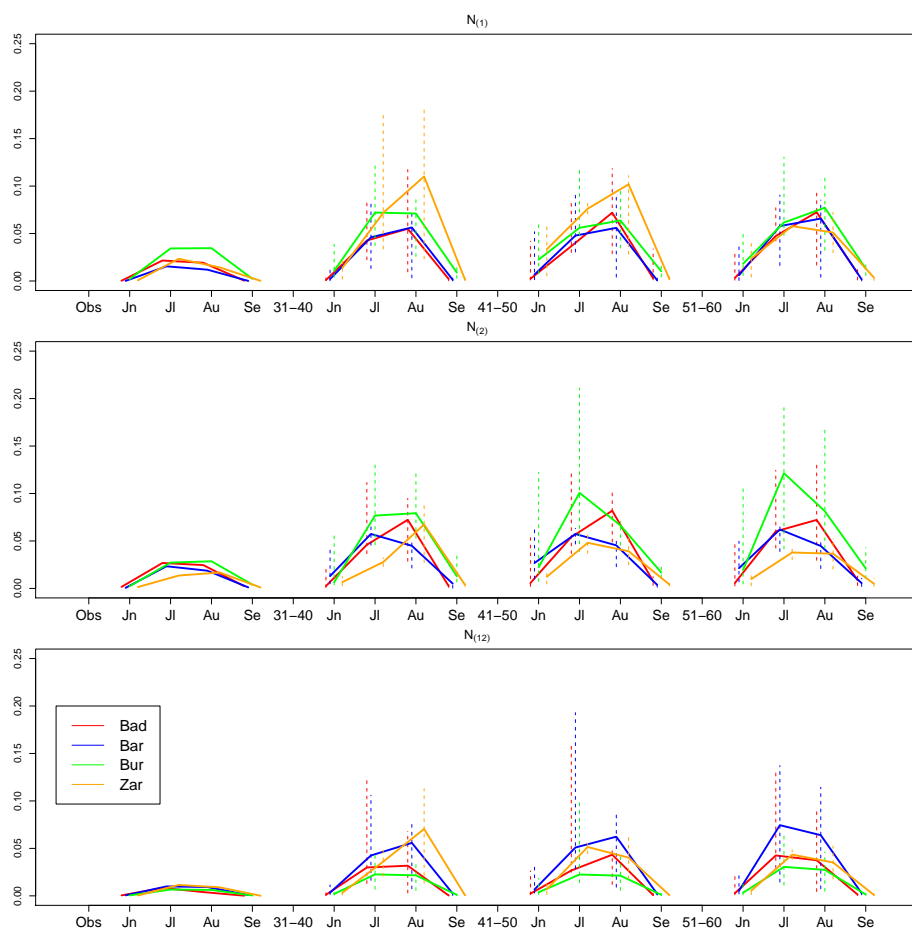


Fig. 8 Seasonal pattern of the observed $\bar{\lambda}_{25}$ and of the $Q2_{\bar{\lambda}_{25}}$ values under RCP4.5 in 2031-40, 2041-50 and 2051-60. Vertical bars show the range of the λ_{25} values used to calculate each median.

401 Zaragoza, where $Q2_{\bar{\lambda}_{25}}$ decreases in August in all type of events, and in $N_{(1)}$ also
 402 in July. The increases are more generalised in September and specially in June.

403 In order to analyse the time evolution of the seasonal pattern, Figure 8 displays
 404 the $Q2_{\bar{\lambda}_{25}}$ in a different way: the monthly patterns in each decade are plotted in
 405 a row, with the observed period in the first place. Locations are displayed with
 406 different colours and the variability within the trajectories is shown by vertical
 407 bars displaying the range of the $\bar{\lambda}_{25}$ values used to calculate each median value.
 408 To make easier comparisons across the types of event and the scenarios, the same
 409 y-scale is used in all the plots in Figures from 8 to 11. A clear increase in the

410 projected values is observed in all the months, locations and types of event, since
 411 $Q2_{\bar{\lambda}_{25}}$ values exceed their observed counterparts in all the cases. The seasonal
 412 pattern does not show relevant differences between the three decades.

413 *Results by type of event*

414 $N_{(1)}$. In 2031-40, the projected increases in Barcelona and Badajoz show a
 415 similar evolution, with a median value in August greater than 0.05, while Burgos
 416 and Zaragoza show a higher increase. In August 2031-50, the $Q2_{\bar{\lambda}_{25}}$ values in
 417 Zaragoza reach 0.1. In the last decade, the $Q2_{\bar{\lambda}_{25}}$ values are similar in all the
 418 locations, with values from 0.047 to 0.062 in July and from 0.051 to 0.077 in
 419 August.

420 $N_{(2)}$. $Q2_{\bar{\lambda}_{25}}$ values in July and August 2031-40 move around 0.05, except in
 421 July in Zaragoza where it is 0.028. The values in 2051-60 show more spatial het-
 422 erogeneity than their counterparts in $N_{(1)}$, with the highest increase in Burgos,
 423 and the lowest one in Zaragoza.

424 $N_{(12)}$. As in $N_{(1)}$ and $N_{(2)}$, the levels of the projections in the three decades are
 425 quite similar. Barcelona shows the highest $Q2_{\bar{\lambda}_{25}}$, over 0.05, in all the months and
 426 decades, except in August 2031-40. Moreover, in 2051-60, $Q2_{\bar{\lambda}_{25}}$ values in $N_{(12)}$
 427 in Barcelona are higher than their counterparts in $N_{(1)}$ and $N_{(2)}$. $Q2_{\bar{\lambda}_{25}}$ values
 428 in Burgos increase with respect to the observed ones, but less than in the other
 429 locations and the other types of events.

430 5.3 Comparison of the projections in 2031-60 under RCP4.5, RCP6.0 and RCP8.5

431 *5.3.1 Evolution of the mean level*

432 The plots of the observed $\bar{\lambda}_{25}$ and the $Q2_{\bar{\lambda}_{25}}$ under RCP6.0 and RCP8.5 are shown
 433 in Figures 9 and 10, respectively. For easier comparison, Figure 11 summarises all
 434 the projections using different symbols for each scenario. The range of the $Q2_{\bar{\lambda}_{25}}$
 435 corresponding to the three scenarios is displayed with dashed vertical lines. In
 436 those figures, the values of $Q2_{\bar{\lambda}_{25}}$ which are calculated with only one trajectory

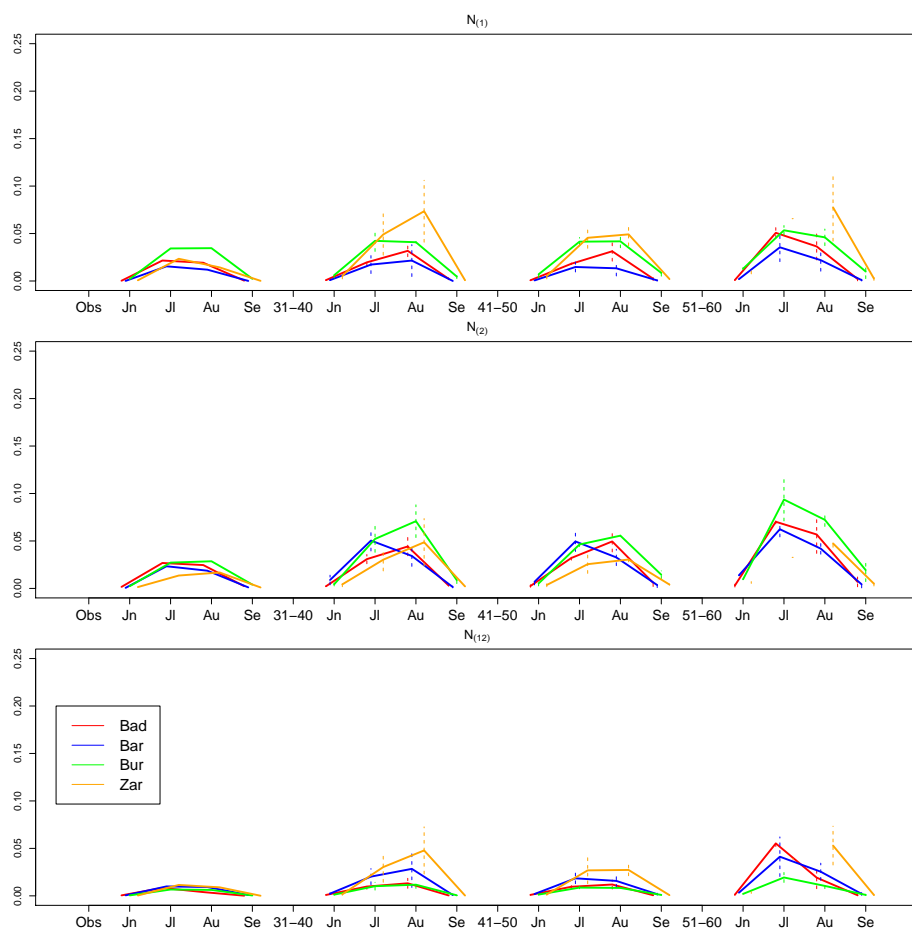


Fig. 9 Seasonal pattern of the observed $\bar{\lambda}_{25}$ and of the $Q2_{\bar{\lambda}_{25}}$ values under scenario RCP6.0, by decade. Vertical bars show the range of the $\bar{\lambda}_{25}$ values used to calculate each median.

437 are not plotted, since they are not real median values. The numerical values shown
 438 in these plots are also summarised in tables, see additional material: file 1.

439 *Scenarios.* The projections under the three scenarios suggest a clear increase in
 440 the mean level of the intensity, with the $Q2_{\bar{\lambda}_{25}}$ values under the three scenarios
 441 higher than the observed $\bar{\lambda}_{25}$. In 2031-50, the projections under RCP6.0 are smaller
 442 than under RCP4.5, as expected due to the evolution of these scenarios. However,
 443 they show a similar growth in 2051-60, except in $N_{(12)}$, where some locations show
 444 slight differences in July and August.

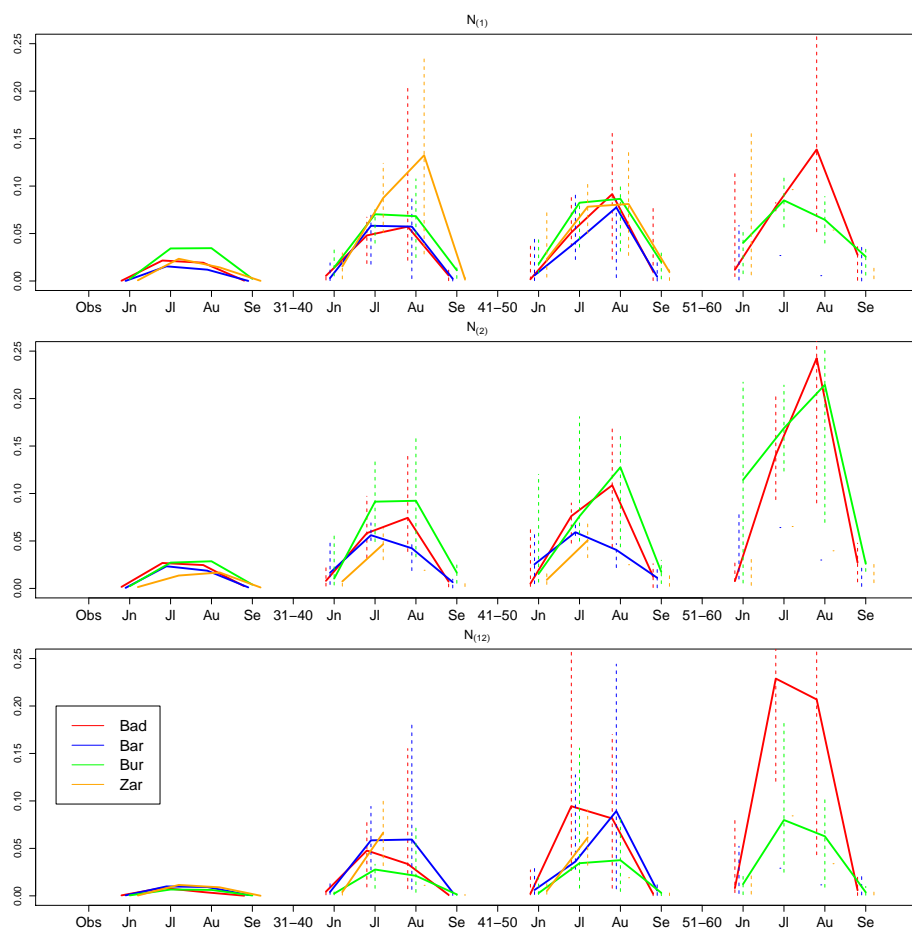


Fig. 10 Seasonal pattern of the observed $\bar{\lambda}_{25}$ and of the $Q2_{\bar{\lambda}_{25}}$ values under scenario RCP8.5, by decade. Vertical bars show the range of the $\bar{\lambda}_{25}$ values used to calculate each median.

445 The evolution under RCP8.5 shows more relevant differences. The first is that
 446 this scenario leads to more extrapolation problems, so that less projections can
 447 be obtained. For example, in July and August 2051-60, only Badajoz and Burgos
 448 have more than one projected trajectory. In 2031-40, similar values are obtained
 449 under RCP8.5 and RCP4.5. However, in 2041-50 the projections grow faster under
 450 RCP8.5, and from 2051 onwards much higher values than in the other scenarios
 451 are projected. The wide range of the $\bar{\lambda}_{25}$ values (represented by the vertical bars)
 452 under RCP8.5 indicates that the ESMs in this RCP show a much higher variability.

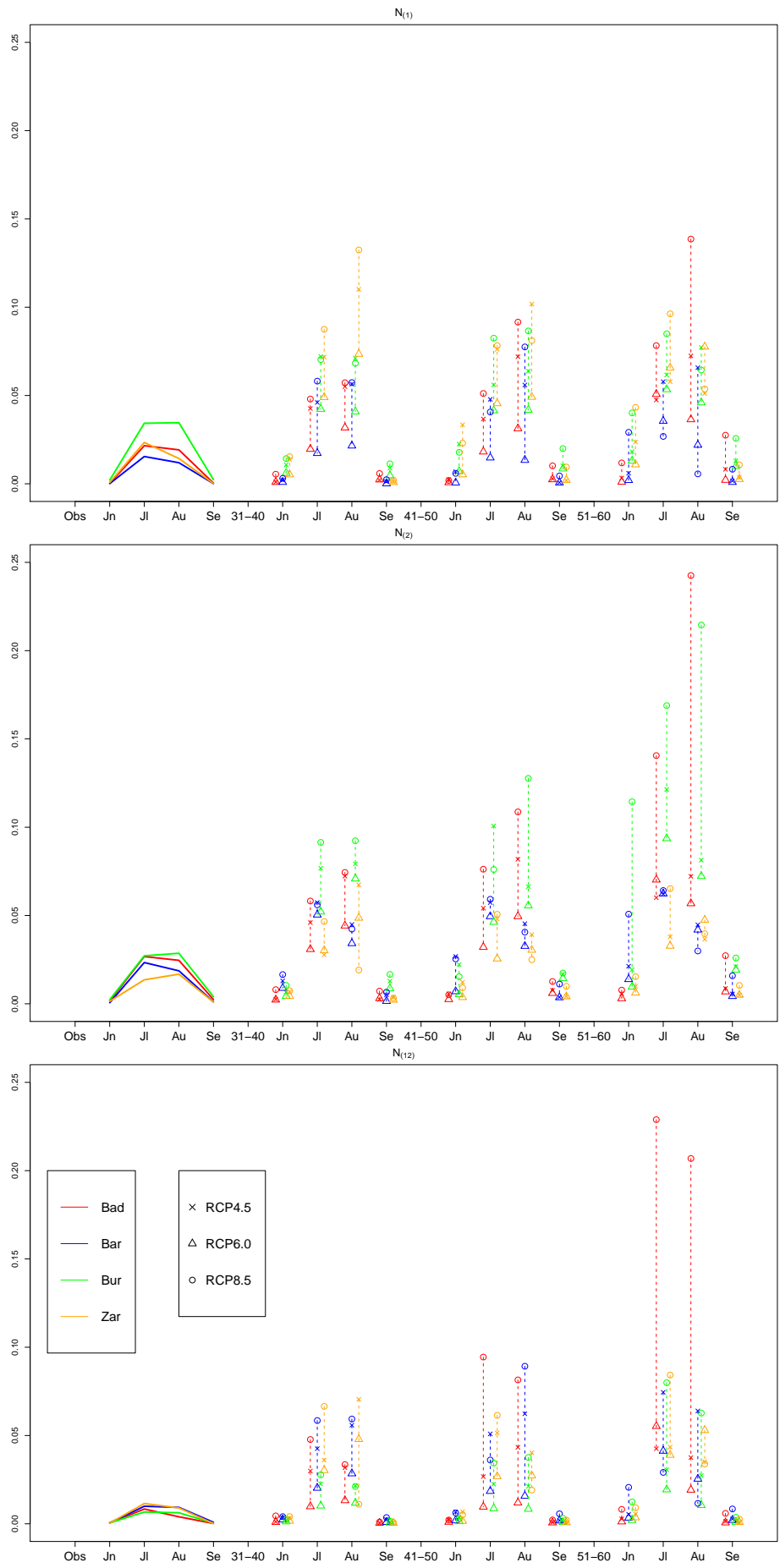


Fig. 11 Observed $\bar{\lambda}_{25}$ and $Q2_{\lambda_{25}}$ by decade and RCP. Vertical bars show the range of the projections under the different RCPs.

453 *Evolution by decade.* In 2031-40 there are few differences between the three RCPs.
454 In all of them the highest intensities in $N_{(1)}$ are projected in July and August in
455 Zaragoza (0.072 and 0.11) and in $N_{(2)}$ in Burgos, (0.077 and 0.079). In $N_{(12)}$,
456 Burgos shows the lowest $Q2_{\bar{\lambda}_{25}}$, around 0.02, and Zaragoza and Barcelona the
457 highest, in all the scenarios.

458 The projections in 2041-50 show more variability between the scenarios. A
459 slight increase is projected under RCP8.5, in $N_{(12)}$ and in some locations in $N_{(2)}$.

460 In 2051-60, the projections under RCP4.5 do not increase their mean level with
461 respect to the previous decades, but around 16% (10 out of 60) of the $Q2_{\bar{\lambda}_{25}}$ values
462 diminish. On the other hand, RCP8.5 projects a high increase in Burgos (except
463 in $N_{(1)}$) and Badajoz.

464 *Seasonal pattern.* The seasonal pattern does not show important changes in any
465 type of event, location or scenario. In all cases, the projections in June and Septem-
466 ber are higher than their observed counterparts, but they do not attain the pro-
467 jected values in July and August. However, in all the events and all the locations
468 except Badajoz, the projections under RCP8.5 in June 2051-60, and sometimes
469 even in previous decades, reach the highest observed values in July and August.

470 5.3.2 Decomposition of the variability of the projections

471 For a given a location, month, decade and type of event, the $\bar{\lambda}_{25}$ values corre-
472 sponding to the available ESM trajectories and the three scenarios are obtained.
473 To analyse the sources of the variability within these sets of projections, we use
474 a sum of squares decomposition considering three factors: Location, Scenario and
475 ESM, the latter nested in the first two. This decomposition is analogous to that
476 performed in an ANOVA model but here it only has descriptive purposes. Similar
477 analyses can be found in Déqué et al (2012), Räisänen and Rätty (2013) and Paeth
478 et al (2017).

479 Since our interest lies in the variability due to the Location and the Scenario
480 factors, Table 5 summarises the percentages of variability explained by them,

Event	$N_{(1)}$		$N_{(2)}$		$N_{(12)}$	
	%LOC	%SCE	%LOC	%SCE	%LOC	%SCE
2031-40						
May	42.3	3	54.3	5.9	57	3.3
June	26.7	9.3	13.1	6.1	14.9	9.7
July	21.6	11.4	26.1	5.3	16.5	13.1
August	19	6.9	29.6	1.7	12.6	6.5
September	36.4	8.5	37.7	5.5	31.2	8.8
2041-50						
May	21.3	2.3	14	5	33	4.2
June	13.4	10.6	10.8	8.1	8.9	7.9
July	18	24.2	22.4	12.5	8.3	9.3
August	9.4	17.6	39.9	11.9	12	18.1
September	13.4	11	17.6	15.7	12.5	19.7
2051-60						
May	28.6	5.6	9.9	6.8	27.2	8
June	7.9	17.9	19.3	11.3	7.4	15.8
July	16.3	9.3	34.1	20	18	23.9
August	17.3	9.3	27.7	24.4	14.6	15.5
September	16.4	23.7	16.3	18.3	9.7	23.4

Table 5 Percentage of variability within the sets of projections explained by the factors Location (%LOC) and Scenario (%SCE).

481 %LOC and %SCE respectively. A low percentage %LOC (%SCE) indicates that
482 the differences between the locations (scenarios) are less relevant than the other
483 sources of variability. Differences between scenarios grow over time, with the me-
484 dian of %SCE equal to 6.9% in 2031-40 and to 15.8% in 2051-60. The main con-
485 clusions are summarised below by type of event.

486 $N_{(1)}$. In the first decade, the projections show differences between locations
487 but they are similar under the three scenarios, with %SCE percentages lower than
488 12%. The projections in all the locations are more similar from 2041, with %LOC
489 values lower than 20% except in May.

490 $N_{(2)}$. The variability between locations is higher in this type of events, with
491 %LOC values greater than 22% in July and August in the three decades and only
492 4 (out of 15) lower than 16%. The variability between scenarios is low, with 12
493 out of 15 of the %SCE values lower than 16%. In July and August, the sum of the
494 variability of both factors increases gradually from the first to the third decade,
495 which is consistent with the values in Figure 11.

496 $N_{(12)}$. The variability between locations is in general low, with all the values
497 lower than 19% except those in May and one in September. The variability between

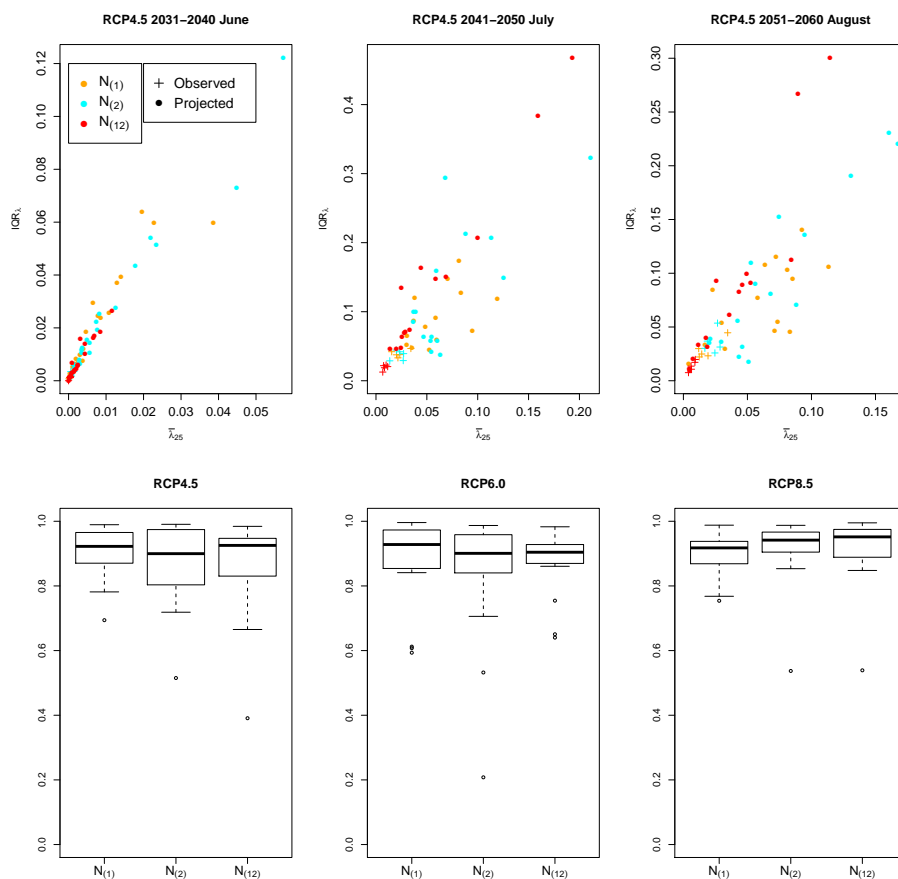


Fig. 12 Plots of IQR_λ versus $\bar{\lambda}_{25}$ for a month in each decade under RCP4.5 (top row) and boxplots of the correlation coefficients between IQR_λ and $\bar{\lambda}_{25}$ under the three RCPs (bottom row)

498 scenarios is also low, with all the %SCE values lower than 20% except in the last
 499 decade, which shows a greater variability.

500 5.3.3 Evolution of the variability of the projected daily intensities

501 In this section, the evolution of the variability of the projected daily intensities is
 502 studied using the interquartile range IQR_λ defined in Section 5.1.3.

503 First, the relationship between the mean level and the variability of the in-
 504 tensities is checked graphically. A strong linear positive relation is found in most

505 cases, see as an example the top row in Figure 12, where the plots of IQR_λ versus
506 $\bar{\lambda}_{25}$, for the three types of events are shown in June 2031-40, July 2041-50 and
507 August 2051-60 under RCP4.5.

508 This linear relationship is quantified using the correlation coefficient. Given
509 the high number of coefficients (around 540=5 months \times 3 decades \times 3 RCPs \times
510 3 types of event \times 4 locations), they are summarised using boxplots by type of
511 event and scenario, see bottom row in Figure 12. The median of the coefficients
512 under RCP4.5, RCP6.0 and RCP8.5 are 0.92, 0.91 and 0.93 respectively, and the
513 first quantiles, 0.84, 0.86 and 0.88. In all the scenarios, more than 82% of the
514 coefficients are greater than 0.8. This high correlation between the mean and the
515 variability suggests that the conclusions of the projected change for the mean level
516 are also valid for the variability.

517 A sum of squares decomposition of the variability of the sets of IQR_λ values
518 (not shown) leads to similar conclusions to those obtained for $\bar{\lambda}_{25}$ in Section 5.3.2.
519 The variability explained by the scenarios is low, lower than 16% in 2031-40. The
520 variability between locations is higher than between scenarios, except in 9 cases
521 out of 45. In general, $N_{(2)}$ shows the highest %LOC values (most of them higher
522 than 23%), and $N_{(12)}$ the lowest.

523 All these results show that the dispersion of the projected daily intensities will
524 be greater than that of the observed intensities, in all the decades and scenarios.
525 Hence, the increase in the mean frequency of EHEs will be accompanied by an
526 increase in the variability of that frequency, so that a very high number of EHEs
527 can be expected in some years during the next decades.

528 5.4 Comparison with other works

529 Projections of high percentiles of Tx_t in summer have been obtained to analyse
530 the future changes in the upper tail of temperature distributions, see for example
531 El Kenawy et al (2015) for a study in the Ebro Valley (NE Spain). However, as
532 far as we know, there are no projections of the occurrence of EHEs in Spain. This

533 section summarises the conclusions drawn in other studies about projections of
534 the occurrence of heat waves in nearby areas, for time periods around mid 21st
535 century. It must be taken into account that they are based on different heat wave
536 definitions, so that a direct comparison is not possible. However, our results are
537 generally consistent with them.

538 Lemonsu et al (2014) carried out a study with a similar objective, the analysis
539 of the temporal evolution of heat wave frequency in the Paris area under A1B,
540 A2 and B1 scenarios for 2020-49 and 2070-99. Their heat wave definition is based
541 on the moving average of daily maximum and minimum temperatures over 3 days
542 and it is applied to RCM projections. They found a systematic increase in the
543 mean number of heat waves: 1 every 7 years during the observed period, 1 every
544 2 years in 2020-49, and between 1 and 2 every year in 2070-99. This means that
545 the projected increase ratio between 2020-49 and the observed period is around
546 3.5. In our case, the median of the projected increase ratios between 2031-40 and
547 1971-2000 in July and August is 3.5 for the simultaneous events, 2.2 for $N_{(1)}$ and
548 2.4 for $N_{(2)}$.

549 Pereira et al (2017) analysed the occurrence of heat waves, defined only with
550 T_x , in 12 locations in the Iberian Peninsula. They compared the observed values in
551 1986-2005 with those projected in 2046-2065 using a RCM forced with MPI-ESM-
552 LR under RCP8.5. They found statistically significant changes in the frequency
553 of occurrence in Barcelona, with a projected/observed ratio of 7.9. Some other
554 locations next to those considered in this paper are also analysed: Cáceres with
555 a ratio of 3.4, Madrid with 3.8 and Sevilla with 3.1. These results are consistent
556 with our projections in 2041-50 for $N_{(1)}$ under RCP8.5, where the ratios in July
557 and August are 2.6 and 6.5 in Barcelona, 2.4 and 4.8 in Badajoz, and 3.3 and 5.7
558 in Zaragoza.

559 Fischer and Schär (2010) analysed future changes in summer heat waves using
560 six RCMs of the ENSEMBLES multi-model experiment with simulations forced
561 with the SRES A1B scenario. They found that in the Iberian Peninsula and the

562 Mediterranean region, the frequency of heat waves per summer will increase from
563 an average of about 0.2 in 1961-90 to around 1.3 in 2021-50, so that the increasing
564 factor is around 6.5. They also studied the frequency of days with $Tx > 35^{\circ}C$
565 and $Tn > 20^{\circ}C$, which is a similar concept to that of simultaneous events. The
566 increasing factor of this frequency between the same periods is 2.3.

567 Lau and Nath (2014) obtained projections of the occurrence and intensity of
568 spatial heat waves in western Europe, including France and Germany but not
569 the Iberian Peninsula, under RCP4.5 and using the GFDL high resolution atmo-
570 spheric model (HiRAM) with 50-km grid spacing. They found that the frequency
571 of heat waves projected in 2026-35 will increase by a factor 3.3 with respect to the
572 frequency observed in 1979-2008.

573 **6 Conclusions**

574 In this work, we propose a statistical model for extreme heat events which can be
575 used to obtain future projections of the occurrence of those events at a daily and
576 local scale. It is shown that the suggested approach is useful to obtain projections
577 at those scales, where the dynamic climate models show difficulties, and which are
578 required in climate change impact studies and other applications.

579 *Occurrence model of extreme heat events.* A non homogeneous common Poisson
580 shock process is applied to jointly model the occurrence of extreme heat events in
581 maximum and minimum daily temperature series in five Spanish locations. The
582 NHCPSP is made up of three conditionally independent Poisson processes which
583 model the occurrence of EHEs only in Tx_t , only in Tn_t and in both temperatures
584 simultaneously.

585 The set of potential covariates in the models includes harmonic terms, short
586 term temperature moving means, Tx_{m15} , Tn_{m15} , Tx_{m31} and Tn_{m31} , polynomial
587 functions of them and interactions with the harmonic terms. The final fitted models

588 are simple, including only one harmonic and linear temperature terms in most
589 cases. All of them are satisfactorily validated.

590 *Projection methodology.* The fitted models are useful for obtaining local projec-
591 tions of the intensity of the EHE occurrence under climate change conditions.
592 These conditions are described by the covariates obtained from the future temper-
593 ature trajectories generated by ESMs, appropriately downscaled to fit the local
594 characteristics. Trajectories from RCMs could also be used.

595 In order to obtain reliable projections, two issues have to be checked. First, that
596 the considered trajectories reproduce adequately the current climate and second,
597 that the models are not used under severe marginal or multivariate extrapolation
598 conditions. Simple tools to check these requirements are provided. This approach
599 has proved to be generally useful for medium-term projections, since four out of
600 the five locations considered passed the extrapolation control.

601 To analyse the projected daily intensities, two summary measures, the 25%
602 trimmed mean $\bar{\lambda}_{25}$ for the mean level, and the interquartile range IQR_{λ} for the
603 variability are suggested.

604 *Results of the EHE projections.* The most relevant feature of the projections in
605 2031-60 is the high increase in the intensities, specially in July and August. The
606 projections in June and September are higher than their observed counterparts in
607 all the cases, but they do not attain the projected values in July and August. How-
608 ever, the projections under RCP8.5 in June in the last decade reach the observed
609 values in July and August, except in Badajoz.

610 Projections under RCP4.5 and RCP8.5 are quite similar in 2031-40, but in the
611 following decades a high increase is projected under RCP8.5, while there is no
612 increase under RCP4.5 nor RCP6.0.

613 It is noteworthy the high increase projected in the occurrence of simultaneous
614 events $N_{(12)}$. Although this type of events shows the lowest intensities in the
615 observed period, it shows the highest ratio projected/observed intensities in 2031-

616 40. More precisely, under RCP4.5 and RCP8.5, the frequency in $N_{(12)}$ in July
617 and August from 2031 onwards will be more than three times higher than in the
618 observed period.

619 Concerning spatial behaviour, RCP6.0 shows the lowest variability of the three
620 scenarios and RCP8.5 the highest. It is also observed that different evolutions
621 are projected in locations with the same Köppen climate classification, such as
622 Badajoz and Barcelona. There is not any spatial pattern, except in $N_{(2)}$, where
623 Burgos shows the highest projected intensities in all the scenarios and decades.

624 The conclusions about the projected change for the mean level of the occurrence
625 intensities are also valid for its variability. This result is determined by the high
626 correlation found between the mean level and the variability summary measures,
627 $\bar{\lambda}_{25}$ and IQR_{λ} .

628 *Future work.* The suggested approach is not useful for obtaining long-term pro-
629 jections of the EHE occurrence due to the extrapolation problem, and even over a
630 medium time horizon it may not be adequate in some cases. We intend to use this
631 type of model with other atmospheric covariates to obtain projections up to 2100.
632 These covariates also reflect the climate change conditions, but they have a lower
633 explicative capacity of the EHE process. Their advantage is that they do not lead
634 to severe extrapolation, unlike the temperature variables.

635 **Acknowledgements** The authors acknowledge the financial support from the Ministerio de
636 Ciencia e Innovación (Spanish Department of Science) and the Ministerio de Medio Ambi-
637 ente (Spanish Department of Environment) through projects CGL2009-09646 and ESTCENA
638 2009/0017. They thank the anonymous reviewers for their helpful comments and AEMET, the
639 Spanish meteorological agency, and specially M^a Jesús Casado for supplying the temperature
640 data.

641 **References**

642 Abaurrea J, Asín J, Cebrián AC, Centelles A (2007) Modeling and forecasting
643 extreme heat events in the central Ebro valley, a Continental-Mediterranean

- 644 area. *Global Planet Change* 57(1-2):43–58
- 645 Abaurrea J, Asín J, Cebrián AC (2015a) A bootstrap test of independence between
646 three temporal nonhomogeneous Poisson processes and its application to heat
647 wave modeling. *Environ Ecol Stat* 22(1):127–144
- 648 Abaurrea J, Asín J, Cebrián AC (2015b) Modeling and projecting the occurrence
649 of bivariate extreme heat events using a non-homogeneous common Poisson
650 shock process. *Stoch Environ Res Risk Assess* 29:309–322
- 651 AEMET (2011) Atlas climático ibérico/Iberian climate atlas. Agencia Estatal de
652 Meteorología, Ministerio de Medio Ambiente y Rural y Marino, Madrid, Insti-
653 tuto de Meteorologia de Portugal
- 654 Amengual A, Homar V, Romero R, Brooks H, Ramis C, Gordaliza M, Alonso S
655 (2014) Projections of heat waves with high impact on human health in Europe.
656 *Global Planet Change* 119(0):71 – 84
- 657 Barriopedro D, Fischer EM, Luterbacher J, Trigo RM, García-Herrera R (2011)
658 The hot summer of 2010: Redrawing the temperature record map of Europe.
659 *Science* 332(6026):220–224
- 660 Beniston M, Stephenson D, Christensen O, Ferro C, Frei C, Goyette S, Halsnaes
661 K, Holt T, Jylhä K, Koffi B, Palutikof J, Schöll R, Semmler T, Woth K (2007)
662 Future extreme events in European climate: an exploration of regional climate
663 model projections. *Climatic Change* 81(1):71–95
- 664 Brands S, Herrera S, Fernández J, Gutiérrez JM (2013) How well do CMIP5 Earth
665 System Models simulate present climate conditions in Europe and Africa? *Clim*
666 *Dyn* 41:803–17
- 667 Casanueva A, Herrera S, Fernández J, Frías MD, Gutiérrez JM (2013) Evaluation
668 and projection of daily temperature percentiles from statistical and dynamical
669 downscaling methods. *Nat Hazard Earth Sys* 13:2080–99
- 670 Cattiaux J, Douville H, Peings Y (2013) European temperatures in CMIP5: origins
671 of present-day biases and future uncertainties. *Clim Dyn* 41(11):2889–2907

- 672 Cebrián AC, Abaurrea J, Asín J (2015) NH-Poisson: An R package for fitting and
673 validating nonhomogeneous poisson processes. *J Stat Softw* 64(6):1–25
- 674 Cheng L, Agha Kouchak A, Gilleland E, Katz RW (2014) Non-stationary extreme
675 value analysis in a changing climate. *Climatic Change* 127(2):353–69
- 676 Coles S (2001) *An Introduction to Statistical Modeling of Extreme Values*.
677 Springer-Verlag
- 678 Déqué M, Somot S, Sánchez-Gómez E, Goodess CM, Jacob D, Lenderink G, Chris-
679 tensen OB (2012) The spread amongst ENSEMBLES regional scenarios: regional
680 climate models, driving general circulation models and interannual variability.
681 *Clim Dyn* 38:951–64
- 682 El Kenawy A, López-Moreno JI, McCabe MF, Brunsell NA, Vicente-Serrano SM
683 (2015) Daily temperature changes and variability in ENSEMBLES regional
684 models predictions: Evaluation and intercomparison for the Ebro Valley (NE
685 Iberia). *Atmos Res* 155:141–57
- 686 Fischer EM, Schär C (2010) Consistent geographical patterns of changes in high-
687 impact European heatwaves. *Nature Geoscience* 3:398–403
- 688 Furrer EM, Katz RW, Walter MD, Furrer R (2010) Statistical modeling of hot
689 spells and heat waves. *Clim Res* 43(3):191–205
- 690 García-Cueto OR, Cavazos MT, de Grau P, Santillán-Soto N (2014) Analysis and
691 modeling of extreme temperatures in several cities in Northwestern Mexico un-
692 der climate change conditions. *Theor and Appl Climatol* 116(1-2):211–25
- 693 Grotjahn R, Black R, Leung R, Wehner MF, Barlow M, Bosilovich M, Gershunov
694 A, Gutowski WJ, Gyakum JR, Katz RW, Lee YY, Lim YK, Prabhat (2016)
695 North American extreme temperature events and related large scale meteorolo-
696 gical patterns: a review of statistical methods, dynamics, modeling, and trends.
697 *Clim Dyn* 46(3):1151–1184
- 698 Gutiérrez J, San-Martín D, Brands S, Manzananas R, Herrera S (2013) Reassessing
699 statistical downscaling techniques for their robust application under climate
700 change conditions. *J Clim* 26:171–88

- 701 Hajat S, Armstrong B, Baccini M, Biggeri A, Bisanti L, Russo A, Paldy A, Menne
702 B, Kosatsky T (2006) Impact of high temperatures on mortality: is there an
703 added heat wave effect? *Epidemiology* 17(6):632–8
- 704 Keellings D, Waylen P (2014) Increased risk of heat waves in Florida: Character-
705 izing changes in bivariate heat wave risk using extreme value analysis. *Applied*
706 *Geography* 46:90 – 97
- 707 Keellings D, Waylen P (2015) Investigating teleconnection drivers of bivariate heat
708 waves in Florida using extreme value analysis. *Clim Dyn* 44(11):3383–3391
- 709 Kysely J, Picek J, Beranová R (2010) Estimating extremes in climate change simu-
710 lations using the peaks-over-threshold method with a non-stationary threshold.
711 *Global Planet Change* 72(1):55–68
- 712 Lau N, Nath M (2014) Model simulation and projection of European heat waves
713 in present-day and future climates. *J Clim* 27:3713–30
- 714 Lemonsu A, Beaulant AL, Somot S, Masson V (2014) Evolution of heat wave
715 occurrence over the Paris basin (France) in the 21st century. *Clim Res* 61:75–91
- 716 Meehl G, Washington WM, Collins W, Arblaster J, Hu A, Buja L, Strand W, Teng
717 H (2005) How much more global warming and sea level rise? *Science* 307:1769–72
- 718 Paeth H, Vogt G, Paxian A, Hertig E, Seubert S, Jacobeit J (2017) Quantifying
719 the evidence of climate change in the light of uncertainty exemplified by the
720 Mediterranean hot spot region. *Global Planet Change* 151:144–151
- 721 Pereira SC, Marta-Almeida M, Carvalho AC, Rocha A (2017) Heat wave and cold
722 spell changes in Iberia for a future climate scenario. *International Journal of*
723 *Climatology* URL <http://dx.doi.org/10.1002/joc.5158>
- 724 Perkins SE, Alexander LV (2013) On the Measurement of Heat Waves. *J Clim*
725 26(13):4500–4517
- 726 Räisänen J, Rätty O (2013) Projections of daily mean temperature variability in the
727 future: cross-validation tests with ENSEMBLES regional climate simulations.
728 *Clim Dyn* 41:1553–68

- 729 Rosenbaum PR (2005) An exact distribution-free test comparing two multivariate
730 distributions based on adjacency. *J R Stat Soc B* 67:515–30
- 731 Sánchez de Cos C, Sánchez J, Jiménez C, Rodríguez E (2016) Using feedback from
732 summer subtropical highs to evaluate climate models. *Atmc Sci Let* 17:230–235
- 733 Smith T, Zaitchik B, Gohlke J (2013) Heat waves in the United States: definitions,
734 patterns and trends. *Climatic Change* 118(3):811–825
- 735 Tobías A, Armstrong B, Gasparrini A, Diaz J (2014) Effects of high summer
736 temperatures on mortality in 50 Spanish cities. *Environmental Health* 13(1):48
- 737 Tryhorn L, Risbey J (2006) On the distribution of heatwaves over the Australian
738 region. *Aust Meteorol Mag* 55:169–82
- 739 Vautard R, Gobiet A, Jacob D, Belda M, Colette A, Déqué M, Fernández J, García-
740 Díez M, Goergen K, Güttler I, Halenka T, Karacostas T, Katragkou E, Keuler
741 K, Kotlarski S, Mayer S, van Meijgaard E, Nikulin G, Patarčić M, Scinocca J,
742 Sobolowski S, Suklitsch M, Teichmann C, Warrach-Sagi K, Wulfmeyer V, Yiou
743 P (2013) The simulation of European heat waves from an ensemble of regional
744 climate models within the EURO-CORDEX project. *Clim Dyn* 41(9-10):2555–
745 2575
- 746 Wang X, Yang T, Shao Q, Acharya K, Wang W, Yu Z (2012) Statistical down-
747 scaling of extremes of precipitation and temperature and construction of their
748 future scenarios in an elevated and cold zone. *Stoch Environ Res Risk Assess*
749 26(3):405–18
- 750 Wilby R, Dawson C (2013) The statistical downscaling model: insights from one
751 decade of application. *International Journal of Climatology* 33(7):1707–19
- 752 Yue T, Zhao N, Fan Z, Li J, Chen C, Lu Y, Wang C, Xu B, Wilson J (2016) CMIP5
753 downscaling and its uncertainty in China. *Global Planet Change* 146:30–37